Building and Environment 230 (2023) 110018

Contents lists available at ScienceDirect

Building and Environment

journal homepage: www.elsevier.com/locate/buildenv

Experimental and numerical evaluation of a novel dual-channel windcatcher with a rotary scoop for energy-saving technology integration

Jiaxiang Li [a,*], John Calautit [a], Carlos Jimenez-Bescos [b], Saffa Riffat [a]

[a] Department of Architecture and Built Environment, University of Nottingham, UK
[b] School of Built and Natural Environment, University of Derby, UK

ARTICLE INFO

Keywords:
Natural ventilation
Windcatcher
Wind tunnel
Computational Fluid Dynamic (CFD)
Energy
Ventilation
Passive cooling
Buildings
Wind flow

ABSTRACT

With the increasing requirements for fresh air supply in buildings after the COVID-19 pandemic and the rising energy demand from buildings, there has been an increased emphasis on passive cooling techniques such as natural ventilation. While natural ventilation devices such as windcatchers can be a sustainable and low-cost solution to remove indoor pollutants and improve indoor air quality, it is not as reliable as mechanical systems. Integration with low-energy cooling, heating or heat recovery technologies is necessary for operation in unfavourable outdoor conditions. In this research, a novel dual-channel windcatcher design consisting of a rotary wind scoop and a chimney was proposed to provide a fresh air supply irrespective of the wind direction. The dual-channel design allows for passive cooling, dehumidification and heat recovery technology integration to enhance its thermal performance. In this design, the positions of the supply and return duct are "fixed" or would not change under changing wind directions. An open wind tunnel and test room were employed to experimentally evaluate the ventilation performance of the proposed windcatcher prototype. A Computational Fluid Dynamic (CFD) model was developed and validated to further evaluate the system's ventilation performance. The results confirmed that the system could supply sufficient fresh air and exhaust stale air under changing wind directions. The ventilation rate of the rotary scoop windcatcher was higher than that of a conventional 8-sided multidirectional windcatcher of the same size.

1. Introduction and literature review

Global warming and fossil-fuel consumption have become the biggest challenges of our times[1]. As one of the biggest carbon dioxide emission contributors, the construction industry is responsible for up to 40% of direct and indirect global carbon emissions [2]. Its energy consumption and carbon emission are expected to grow to 50% by 2050 [3]. Due to the recent pandemic, the concerns for indoor air quality have intensified, and it has been established that increasing the fresh air supply can mitigate the spread of the virus [4]. However, increasing the ventilation rates could increase the heating, cooling and moisture load of air conditioning systems, a major contributor to building energy use, depending on the climatic conditions and requirements for the indoor environment.

The heating, ventilation and air-conditioning (HVAC) system, which is necessary for providing thermal comfort, could account for up to 50% of the building's energy consumption [5]. Moreover, according to the International Energy Agency [6], 10% of global electricity was used for cooling in 2016. The proportion of summer cooling load could reach 40% of the total energy load in areas with hot climatic conditions, such as Shanghai [7]. Without rethinking the conventional HVAC paradigm in buildings, the energy cost of operating them would significantly increase. Thus, many researchers are looking into low-cost solutions for providing building ventilation and indoor thermal comfort [8]. Solutions such as natural ventilation can provide passive cooling and indoor pollutant and moisture removal in buildings without the energy cost [9].

In areas with unfavourable outdoor conditions, such as in hot and dry climates, natural ventilation system alone is typically insufficient to provide thermal comfort because of the high outdoor temperature and humidity in both daytime and nighttime [10,11]. In cold or temperate climates such as the UK, improving the energy efficiency of the building fabric is often considered the most important approach for improving energy use [11]. However, the improved insulation and airtightness could lead to poor indoor air quality. While using natural ventilation during the heating season could lead to ventilation heat loss [12]. Developing a natural ventilation system combined with passive or low-energy heating, cooling and dehumidification technologies can

* Corresponding author.
E-mail address: Jiaxiang.li@nottingham.ac.uk (J. Li).

https://doi.org/10.1016/j.buildenv.2023.110018
Received 27 October 2022; Received in revised form 23 December 2022; Accepted 13 January 2023
Available online 16 January 2023

Abbreviations

ASCD	Anti-short circuit device
CFD	Computational Fluid Dynamic
EAHE	Earth-Air Heat Exchanger
HVAC	Heating, ventilation and air-conditioning
PPM	Parts per million

extend its operating period and enhance the energy-saving potential [13].

A good example of an effective natural ventilation device is the windcatcher, which was used in the Middle East for thousands of years [14]. The windcatcher is installed on the top of the building or roof to provide fresh air into the room by capturing the wind at the windward side with positive pressure. Such a rooftop ventilation system can provide good airflow rates comparable to mechanical ventilation systems [15]. Traditional rooftop windcatchers with one opening to induce the wind flow has to be operated with other openings such as vents or windows [16]. While windcatchers with multiple openings could provide supply and exhaust ventilation with a higher ventilation efficiency than a single-opening system [17]. In multiple opening windcatchers, the polluted air could also be extracted from the room via the windcatcher leeward side or side openings, under negative pressure [8]. A comparison of conventional windcatchers is shown in Table 1. The passive/low-energy technology integration and the advantages and disadvantages of the windcatchers were also compared.

Applying low-energy and passive cooling technologies in conventional windcatchers can enhance their performance by incorporating evaporative cooling, heat pipes and thermal mass. In regions with hot and dry climates, evaporative cooling can effectively reduce the supply airflow temperature [27–29]. The windcatcher can also be combined with a solar wall to increase the ventilation rate [20]. The windcatcher can also be integrated with an Earth-Air Heat Exchanger (EAHE) [30] or a heat transfer coil with a low-temperature heat sink to precool the supply air [31]. Wind direction is an important factor that influences the operation of these systems and can limit ventilation or thermal performance, if not considered. For example, the integration of passive cooling technologies into the windcatcher channel must consider the air channel's change of airflow direction [14,32].

The wind direction influences the pressure differential across the openings of the natural ventilation system, which in turn affects the supply and exhaust of airflow [33]. For those conventional windcatchers integrated with passive technologies, both the ventilation and cooling performance of the windcatcher system could decrease significantly under changing wind directions or even react against the design purpose, as shown in Fig. (1). Fig. (1) presents one of the problems caused by the changing wind directions around a multi-directional windcatcher observed in previous research [34,35]. Adding the cooling device in the windcatcher's front side channel would be beneficial when the wind flow is from the same side. But the cooling devices are no longer effective if the wind is in the opposite direction or changed by 90°.

Some of the evaporative cooling systems had to be assisted by a fan to avoid the impact of changing wind directions [36]. And some of the research employed a rotary windcatcher so that its inlet faces the wind constantly to solve the problem of changing wind directions [16,37]. Additionally, in regions with dry climates, the water resources are limited, and the wastage of water caused by inefficient passive cooling should be avoided [38].

The wind scoop, which is also called the pressure cowl, has a rotary inlet opening which ensures that it faces the wind from all directions to make sure the ventilation performance would not be affected by the changing wind directions and it could be placed at higher locations to capture the wind with high wind speed, such as above the building [39]. An example of a wind cowl installed in 1991 in the ICI chemicals visitor centre in Runcorn, UK, was analyzed [40]. The ventilation performance of the traditional windcatcher decreased dramatically when the wind direction changed and the ventilation efficiency decreased by 50% in the two-side windcatcher and 40% in the three-side windcatcher [41]. Compared with the traditional windcatchers with multiple openings, the wind scoop could provide a stable fresh air supply for passive ventilation, cooling and heating technologies under changing wind directions.

Thus, this research aims to develop and evaluate a novel windcatcher design with a fixed airflow direction inside the system to provide stable ventilation under changing wind directions. The design incorporates a dual-channel design for further integration of passive heating, cooling, dehumidification and heat recovery technologies. Several objectives of this research were achieved, including (1) developing the scaled windcatcher prototype and evaluating the ventilation performance in an experiment, (2) developing the CFD windcatcher model according to the prototype in the experiment and validating the CFD model with the experiment results, and (3) performance evaluation of the proposed windcatcher and comparing its performance against convetional systems and building regulations.

Thus, the dual-channel wind scoop windcatcher was developed with an inlet to supply the air and an outlet to extract the air from the room. The wind scoop windcatcher geometry with two concentric ducts and an airflow diagram is shown in Fig. (2). A rotary wind scoop was applied to the outer duct with a hole in the middle to allow the return duct to pass through. A vertical tail fin on the back generated the torque to rotate the wind scoop and face the wind. The outer duct will constantly be the supply duct with the positive pressure generated from the wind scoop, for the passive technology integration. The chimney in the middle would then extract the stale air out from the building, making the inner duct the constant return duct. Overall, the supply and return positions were fixed and adjacent, no matter how the wind direction changed. On the

Table 1
Comparison of conventional windcatchers with the proposed system in terms of natural ventilation and passive technology integration.

Windcatcher type	Sensitivity to wind direction	Passive or low-energy technology integration	Advantages	Disadvantages
Single-sided windcatcher /Wind tower [16]	High	• Earth-air heat exchanger [18]	Low capital and maintenance cost	Sensitive to wind direction
Two-sided windcatcher [19]	High	• Evaporative cooling spray or cloth [20]	High ventilation rate at design wind direction	Sensitive to wind direction
Four-sided windcatcher [21,22]	Middle	• Heat pipe for cooling and heat recovery [23,24] • Thermal wheel [25]	Good ventilation performance, Passive technologies applied	Integrated passive technologies are sensitive to wind direction
Eight-sided or more openings windcatcher [26]	Low	None	Not sensitive to wind direction	Lower ventilation rate, Challenging integration with passive technologies
Proposed rotary scoop windcatcher	None	• Heat recovery • Heat pipes	Not sensitive to wind direction, Passive technologies and heat recovery can be applied	No existing research and products in the market, Higher capital and maintenance cost

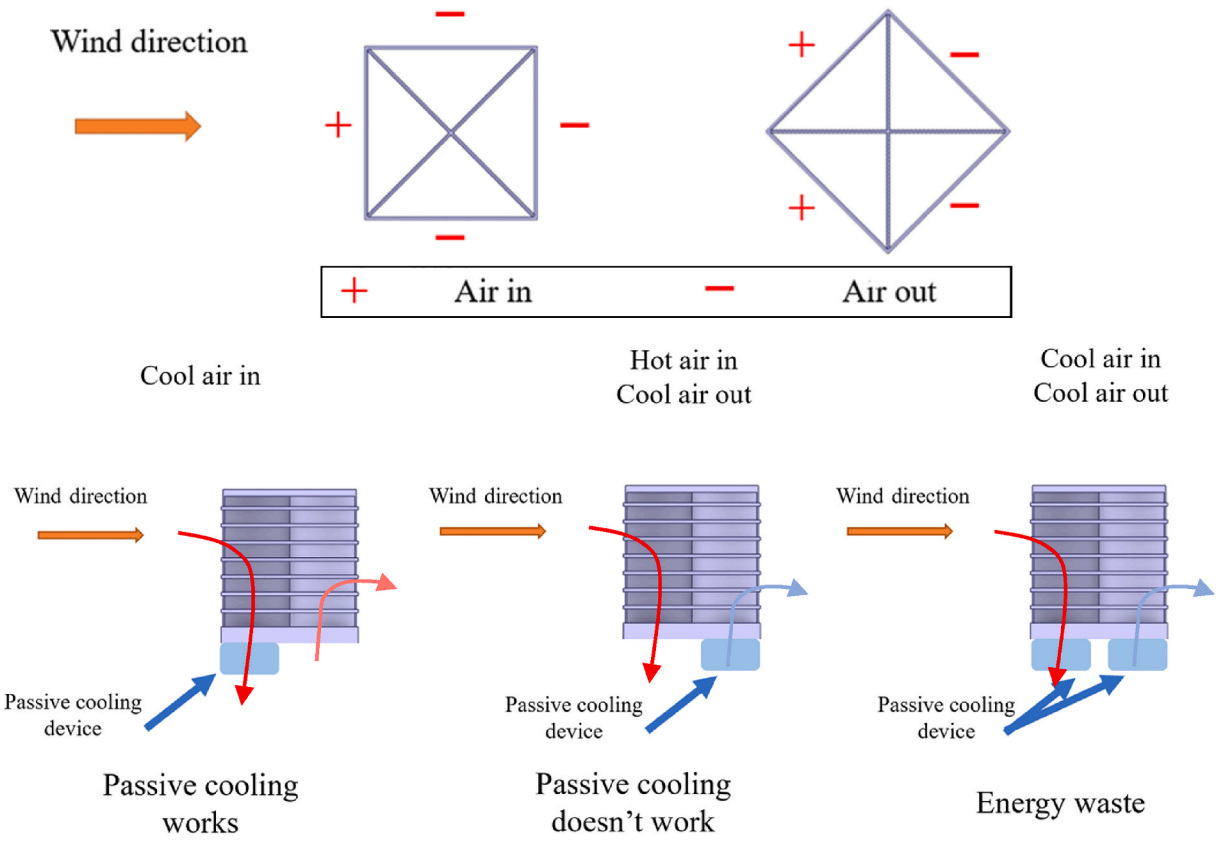

Fig. 1. Conventional windcatcher with a cooling device under different wind directions.

contrary, the windward side in a traditional multiple openings windcatcher will be supplying the fresh air, and the rests would become return ducts which will change with the wind direction. As the supply and return duct were constantly adjacent to each other in the scoop windcatcher and the airflow direction would not change in operation, the energy can be recovered from the return air to the supply air stably and continuously in a passive heat recovery configuration such as heat pipes (see Appendix Fig. A1 and A2).

2. Experimental setup and windcatcher prototype development

The research method is summarized in Fig. (3). A scaled experimental prototype was designed and constructed. The experiment evaluated the ventilation performance first, and the CFD model development and validation were conducted after obtaining the experiment results. The full-scale CFD model was modified from the validated scaled model, and the ventilation performance was compared to the conventional windcatcher and building regulations.

The prototype of this windcatcher contained the rotary wind scoop and ductwork. The rotary scoop was made of stainless steel, and the supply and return ducts were made of transparent acrylic tubes. The vertical tail fin was made of a wood bar and foam board. A ring-shaped bearing connected the rotary scoop and duct to let the supply air pass through the opening. The wind scoop was supported by the ring-shaped bearing connected to the external tube for rotation.

The location of the experimental research was Dalian, China. The experiment was carried out in an enclosed space. In this research, a test room was made to simulate a roof windcatcher installed in a building for ventilation evaluation. A 1.2 m × 1.2 m cube shape test room was made using insulation panels and steel beam structures, as shown in Fig. (4). Six 50 mm thickness insulation broads were used to construct the wall, roof and floor with an internal space of 1.331 m^3. The return duct was extended by 0.5 m to increase the distance between the outlet opening in the room and the position of the hot-wire anemometer. This is to decrease the wind speed difference between the measuring point in the middle and the region close to the tube.

An anti-short circuit device (ASCD) was applied in the test room below the windcatcher to improve the airflow distribution [42]. Two 400 mm L-shape ASCD redirected the flow of supply air from vertical to horizontal. The ventilation performance of the windcatcher with and without ASCD was evaluated by CFD simulation. After applying the ASCD as shown in Fig. (5), less than 1% of the air escaped the building without circulating inside the room while most of the air would leave the building directly if the ASCD was not applied. The airflow distribution in the building was more uniform after applying the ASCD, and the streamline was separated into different directions rather than flowing together.

The mass flow rate at 5 m/s outdoor wind velocity in the model with and without ASCD was 0.1484 kg/s and 0.1496 kg/s, separately. Only a small decrease within 1% occurred after adding the ASCD. Thus, adding the ASCD was useful to provide better air circulation inside the room without significantly decreasing the ventilation performance of the windcatcher. The ASCD would also benefit the integrated passive technologies in the windcatcher by preventing the cooled or dehumidified air leaving the building directly rather than circulating inside the room.

An open wind tunnel was constructed to simulate a stable wind around the windcatcher. A 700W fan was used, and this was connected to a flexible tube with a length of 3 m and a diameter of 0.8 m. A metal contraction was applied to transfer the diameter from 800 mm to 400 mm. The screen mesh, honeycomb and flow conditioner were applied before the opening to stabilize the wind [43].

The components in the open wind tunnel are shown in Fig. (6). The thickness of the wire in the mesh was 0.1 mm, and the gap was about 0.3 mm. The length of the flow conditioner was about 200 mm with a diameter of 10 mm. The initial wind from the fan had a relatively low wind speed in the middle than the surroundings, so a block ring was

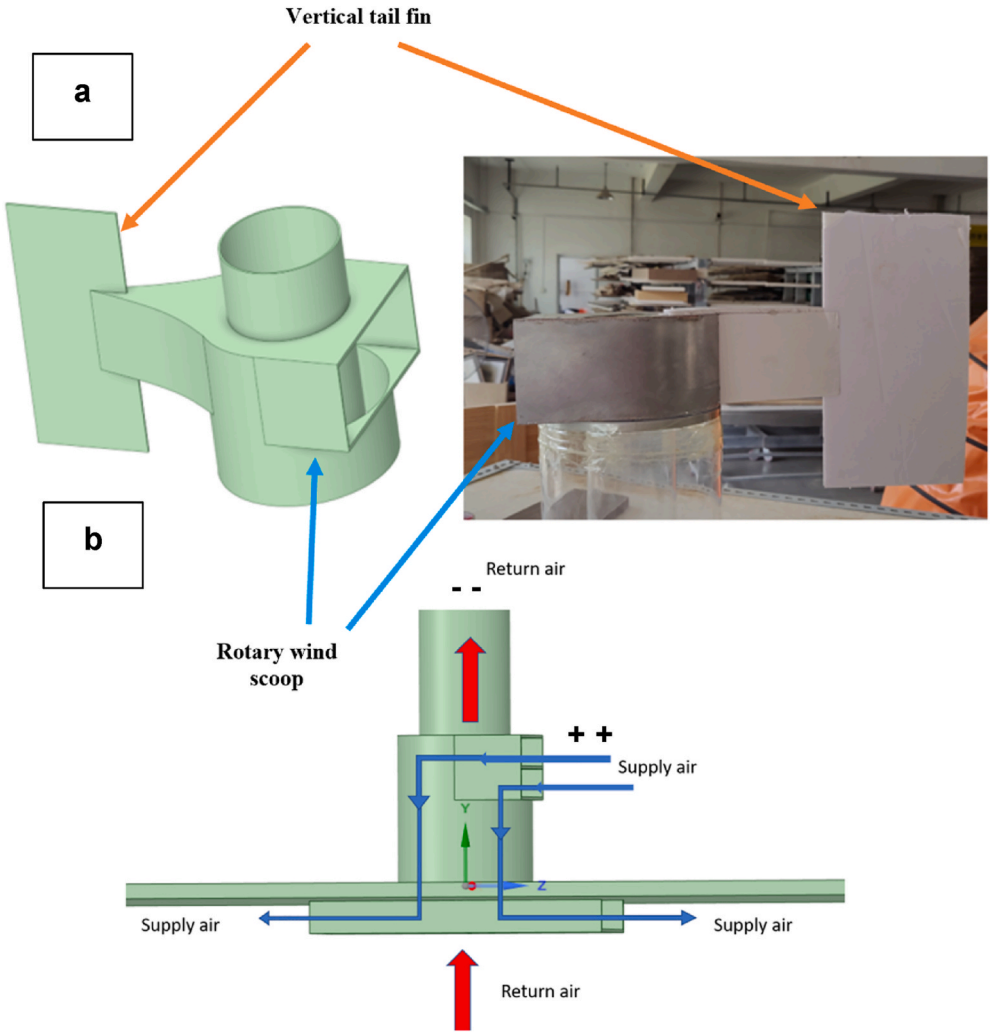

Fig. 2. (a) Proposed rotary windcatcher components, (b) supply and return airflow directions in the windcatcher and ventilated space.

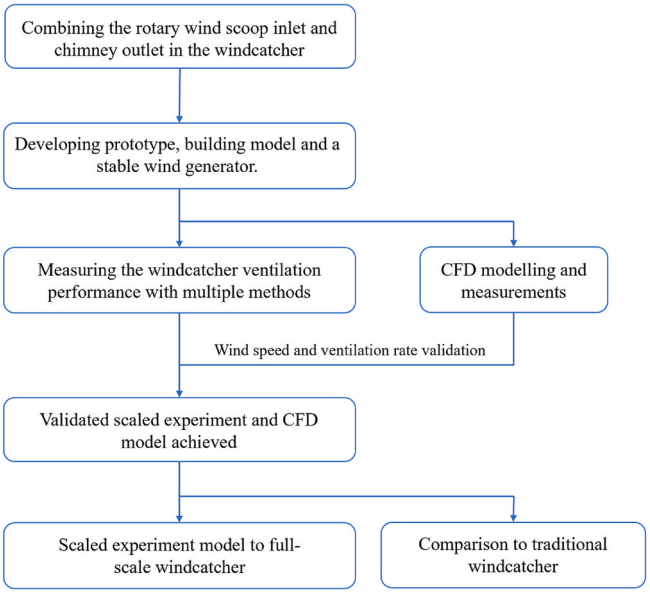

Fig. 3. Research method for the development and evaluation of the dual-channel wind scoop windcatcher device.

added in the middle to let the supply air pass through the middle, closing the gap in wind speed between the middle and surroundings. The difference in wind speed between the middle and surroundings was not perfectly solved, but the uniformity of wind speed was improved to a level sufficient for experimental measurement and result validation.

Wind speeds were measured at 17 points at the open wind tunnel outlet, as shown in Fig. (6), and the wind speed profile was used in the CFD model validation. Because the screen mesh and flow conditioner would increase the system's pressure loss, the maximum wind speed generated was 3 m/s. The average wind speed value of each point was obtained after the wind flow stabilised to eliminate the impact of instant wind speed fluctuation. The voltage of the fan was adjusted to change the wind speed and the wind speed profile in each test was measured to achieve the actual wind speed profile under different average wind speeds. The Testo 405i anemometer was used for wind speed measurement with an accuracy of $\pm$ (0.1 m/s $\pm$ 5% of the readings) .

A 42 cm high, 48 cm long vertical tail fin was added to the back of the rotary wind scoop at a distance of 12 cm from the wind scoop. The rotation of the windcatcher was tested at different wind speeds. A digital camera was used to record and evaluate the movement of the device. Because of the prototype manufacturing limitations, the windcatcher model for the ventilation rate validation, in Fig. (8) and (9)(a), and the rotation test, in Fig. (7) and (15), were slightly different. The extended part of the chimney was removed for the prototype used in the rotation test. It should be noted that the model for the ventilation rate validation was fixed and fully airtight with high friction between the wind scoop

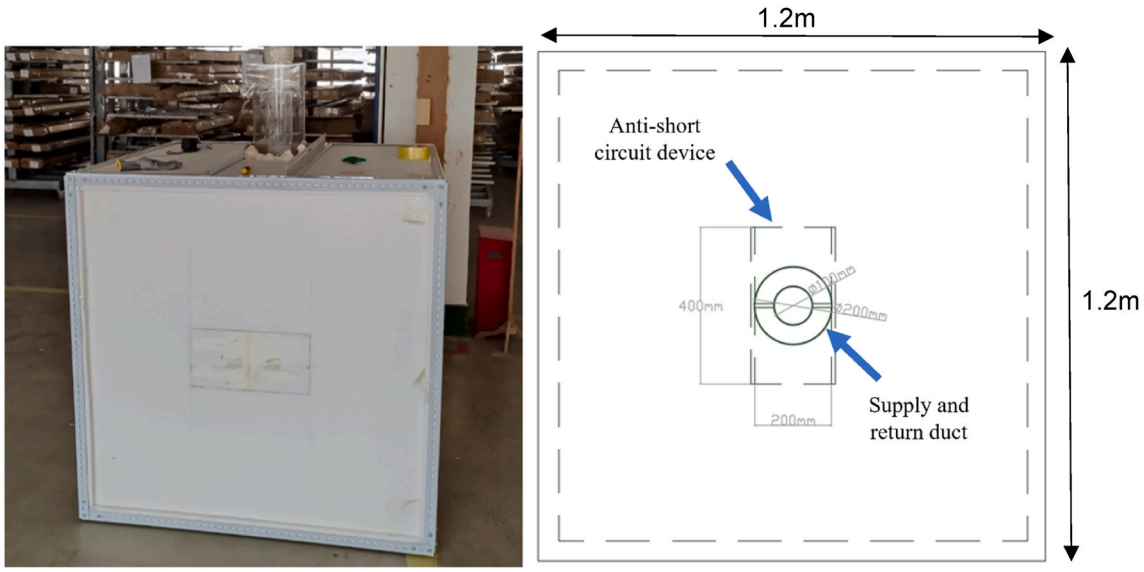

Fig. 4. Experimental test room model showing the integration of the windcatcher and ASCD.

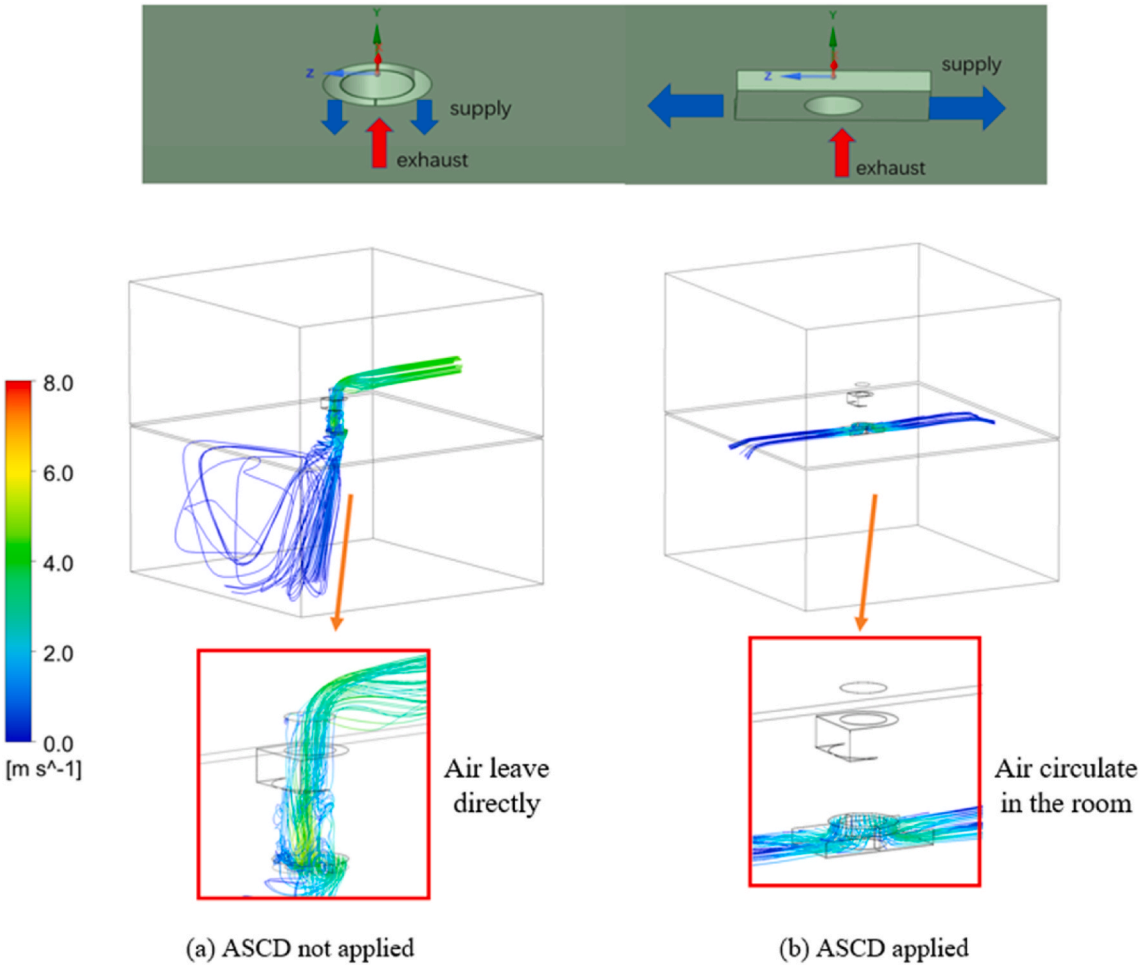

Fig. 5. Anti-short circuit device impact on supply and exhaust airflow.

and chimney, which will prevent it from rotating. Thus, the chimney in the rotary test was slightly lower than the wind scoop to avoid friction and let the model rotate under the wind. This will be addressed in future works by using a different manufacturing technique to further optimize the prototype.

The tracer-gas decay method was used to measure the airtightness of the sealed test room with low pollutants and environmental effects [44]. Carbon dioxide was selected as tracer gas because of its nontoxic

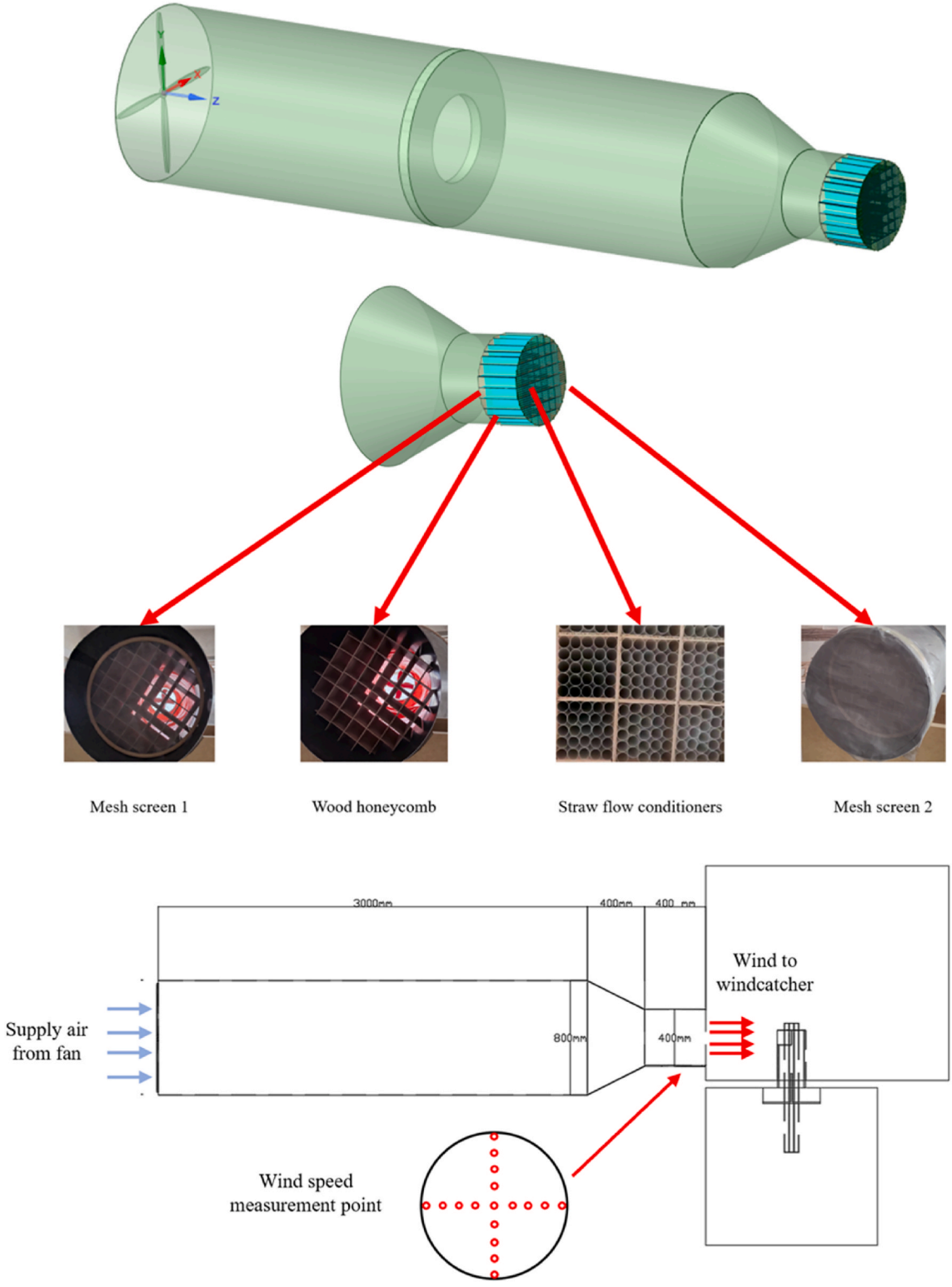

Fig. 6. Open wind tunnel specification and wind catcher setup.

physical properties, and the CO_2 concentration sensor (HTI HT2000) was used to measure the CO_2 concentration. The accuracy of concentration measurement at the condition below 5000 PPM was ± 50 PPM ± 5% of the readings. The carbon dioxide concentration measurement points are shown in Fig. (12). The carbon dioxide sensor was placed in the middle and side of the test room. In the ventilation rate test, the carbon dioxide concentration at the outlet is used for the air change rate calculation.

The air change rate of the test room was calculated by the CO_2 concentration change rate using equations (1) and (2) [45].

$$C(t) = (C(0) - C(e)) \times e^{-Qt/V} + C(e) \quad (1)$$

$$n = Q/V \quad (2)$$

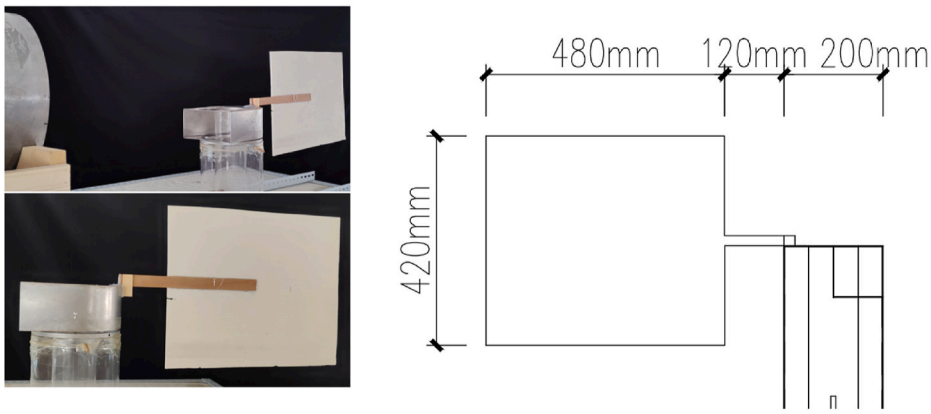

Fig. 7. Windcatcher prototype model in the open wind tunnel testing.

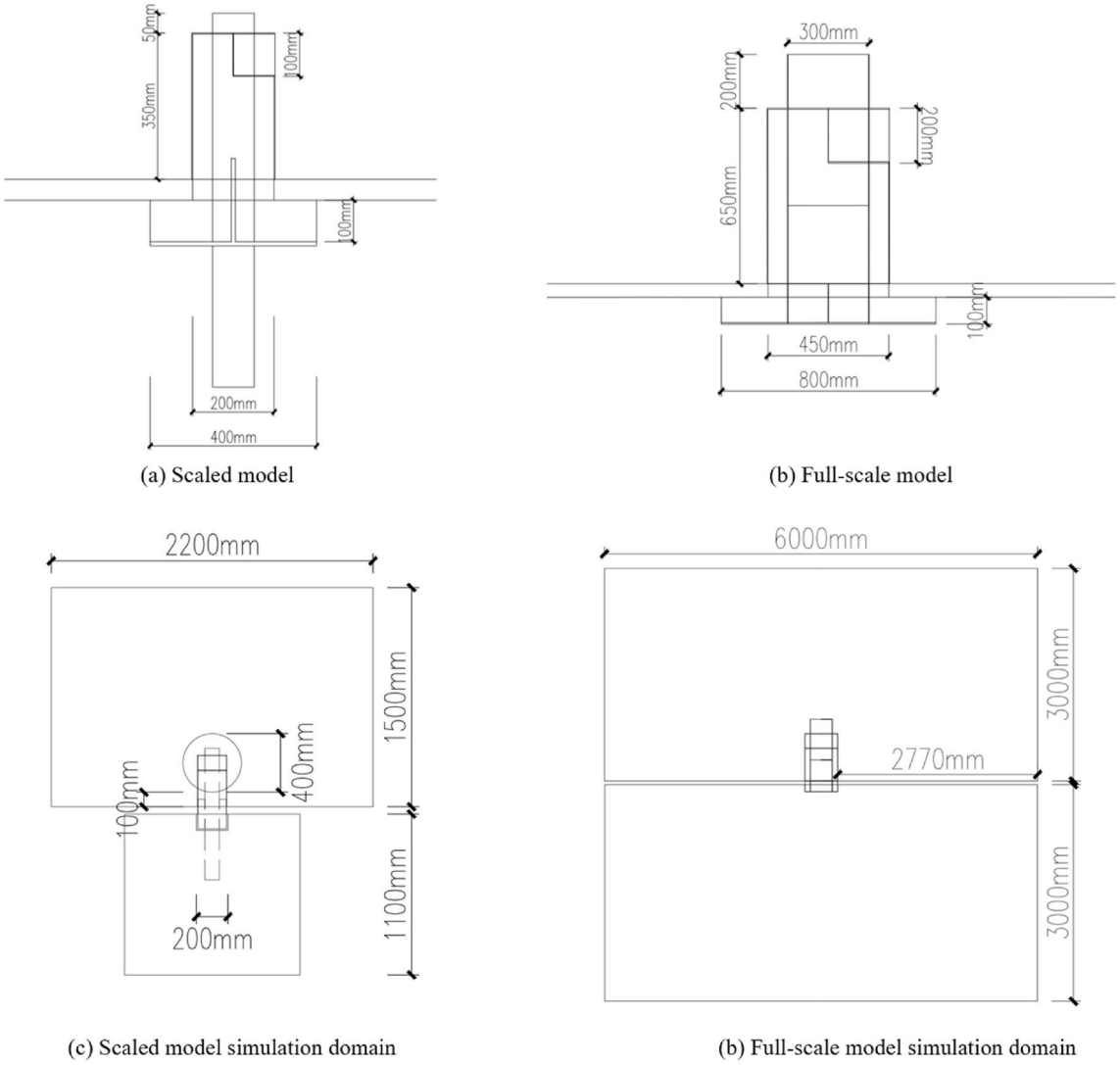

Fig. 8. Dimensions of the scaled (validation), full-scale windcatcher and simulation domain.

where.

$C(t)$ is the CO_2 concentration after t seconds in PPM;
$C(0)$ is the CO_2 concentration at the initial condition in PPM;
$C(e)$ is the CO_2 concentration of the environment in PPM;
Q is the supply air volume flow rate in m^3/h;
V is the internal volume of the test room in m^3;
t is the time in s;
n is the air change rate in h^{-1}.

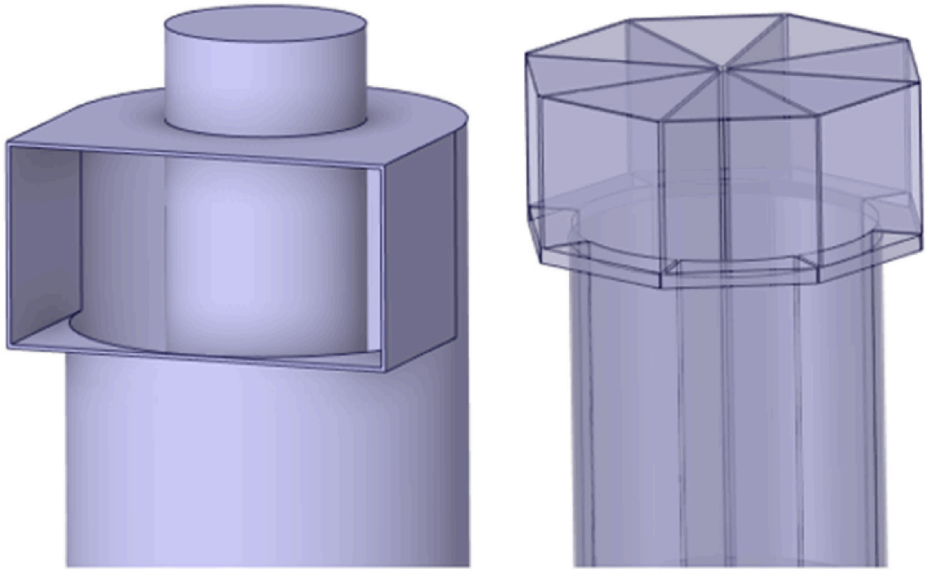

Fig. 9. Geometry of the rotary scoop with central chimney windcatcher and 8-sided windcatcher [48].

In the airtightness measurement, after sufficient time to mix the CO_2 and the indoor air, the initial CO_2 concentration was 3350 PPM, and the final CO_2 concentration was 3200 PPM. The time of air exchange was 3050s and the environment CO_2 concentration was 500 PPM. The air change rate was 0.0625 h^{-1} and the air leakage was 0.023L/s which was ignorable compared to the wind-forced ventilation. Thus, the test room can be treated as an airtight box in the experiment.

3. CFD method

The present work will use Computational Fluid Dynamic (CFD) simulation to further evaluate the performance of the proposed system. The commercial software FLUENT was used for the airflow simulation. The model was created in the 3D modelling software Space Claim in Ansys Workbench. The mass and momentum equations are solved for the airflow in this model. The energy governing equation was not applied as the heat transfer was not investigated in the present study. The Reynolds-averaged Navier-Stokes-based k-epsilon turbulence model was employed[46]. A second-order upwind scheme was employed to discretize all the transport equations. The semi-implicit method for pressure-linked equations segregated pressure-based algorithm solver was applied for the simulation. The governing equations for the mass (eqn. (3)), momentum (eqn. (4)), and k and epsilon (eqns. (5) and (6)) [47] are detailed below:

$$\frac{\partial \rho}{\partial t} + \nabla \times (\rho u) = 0 \tag{3}$$

where u refers to the fluid velocity vector, t is time, and ρ is density.

$$\frac{\partial \rho}{\partial t} + \nabla \times (\rho u \nabla u) = -\nabla p + \rho g + \nabla \times (u \nabla u) - \nabla \times \tau_t \tag{4}$$

where g is a vector of gravitational acceleration, p is the pressure, τt is the divergence of the turbulence stresses, and μ is dynamic molecular viscosity.

$$\frac{\Delta}{\delta t}(\rho k) + \frac{\delta}{\delta x_i}(\rho k u_i) = \frac{\delta}{\delta x_i}\left(a_k \mu_{eff} \frac{\delta k}{\delta x_j}\right) + G_k + G_b - \rho\varepsilon - Y_M + S_k \tag{5}$$

$$\frac{\Delta}{\delta t}(\rho\varepsilon) + \frac{\delta}{\delta x_i}(\rho\varepsilon u_i) = \frac{\delta}{\delta x_j}\left(a_k \mu_{eff} \frac{\delta\varepsilon}{\delta x_j}\right) + C_{1\varepsilon}\frac{\varepsilon}{k}(G_k + C_{3\varepsilon}G_b) - C_{2\varepsilon}\rho\frac{\varepsilon^2}{k} - R_\varepsilon + S_\varepsilon \tag{6}$$

where *Gb* and *Gk* represent the generation of turbulence kinetic energy due to buoyancy and mean velocity gradients. *YM* defines the overall dissipation rate. *αk* and *αε* are the inverse effective Prandtl numbers for *k* and ε. *Sk* and *Sε* are user-defined source terms.

The sizes of the windcatcher model and simulation domain are compared in Fig. (8). It should be noted that the extended return duct was removed in the full-scale model as it's designed for the experimental measurement and may slightly decrease the ventilation performance.

In the CFD validation model (Fig. 8a), the full wind tunnel geometry was not included in the simulation, and instead, a circular inlet was modelled to simulate the outlet of the open wind tunnel. Only the region around the windcatcher and inside the room was simulated in the CFD model to simplify the simulation. The inlet wind speed profile measured from the experiment was applied in the simulation first to validate the CFD simulation model. After validating the simulation model, the inlet wind speed boundary condition was applied to the entire rectangular area as shown in Fig. 8c to simulate the approach wind flow. The ventilation performance of the rotary scoop windcatcher was also compared with a conventional eight-side windcatcher which also had the function of providing fresh air under changing wind directions, see Fig. (9).

For the mesh sensitivity analysis, three mesh sizes were generated and simulated. The ventilation performance difference between the three mesh sizes was ignorable, with an average difference of 0.5% (Fig. 10). The R^2 values of the results for all the mesh sizes were higher than 0.999. The meshing element size of the flow region was 0.008 m, and the face sizing on the windcatcher surface was 0.004 m in the fine mesh. The final mesh node number was 4.22 million, and the elements were 2.48 million. Details of the CFD settings and boundary conditions are summarized in Table 2.

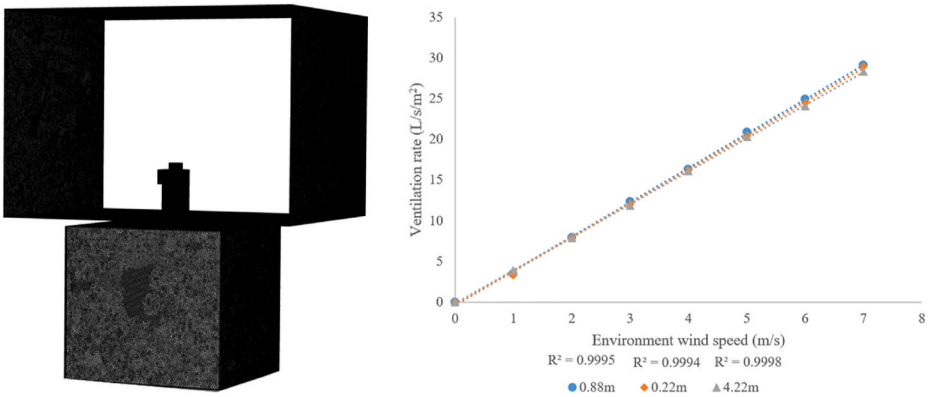

Fig. 10. The surface mesh around of the windcatcher and room model, and the mesh independence analysis results.

Table 2
CFD settings and boundary conditions in the simulation.

Term	Value and selections
Inlet	
Velocity (m/s)	1-7 (uniform wind condition)
Initial Gauge Pressure (Pa)	0
Specification Method	K-Epsilon
Turbulent Kinetic Energy (m^2/s^2)	1
Outlet	
Gauge Pressure (Pa)	0 (atmospheric)
Wall	
Shear Condition	No slip
Roughness Models	Standard
Roughness Height	0
Roughness Constant	0.5
Converged residuals	
Continuity/k/Epsilon	0.001
X/Y/Z velocity	0.0001

4. Experimental and numerical results and discussion

4.1. Validation of the CFD model

In Fig. (11)(a), the y-axis is the distance between the wind speed measure point and the centre of the wind tunnel and the x-axis is the wind speed. As shown in Fig. (11) (a), the wind speed profile is a quadratic function of the distance to the centre of the wind tunnel outlet. The velocity in the middle was slightly lower than the surroundings and the wind speed on the edge was lower because of the friction of the system. With the increase in average wind speed, the gap between the maximum and minimum windspeeds would also increase. The equation of the wind speed profile is detailed in the Appendix. The error range of the wind speed was determined by the percentage calculated from the hotwire anemometer sensors' accuracy based on the manufacturer's calibration.

The CFD model validation was achieved by three methods, including the wind speed profile in the return duct in Fig. (11) (b), the wind speed in three validation points in Fig. (12) and the ventilation rate measured by the wind speed experiment and the carbon dioxide concentration change rate in Fig. (13) and (14). The wind speed profile in the return duct in the CFD simulation and experiment could match each other very well as shown in Fig. (11)(b). In Fig. (11)(b), the y-axis is the distance between the wind speed measure point and the centre of the return duct and the x-axis is the wind speed. Thus, the relationship between the centre wind velocity to the average wind velocity in the return duct was obtained, and the ventilation rate was calculated. The correlation factor of average velocity to centre velocity was a function of the centre wind speed as the wind speed would have an impact on the Reynolds number and the development of airflow inside the tube.

The approximation formula of the velocity in this experiment is shown in Equation (7):

$$\overline{V} = (0.9627 - 0.022 \times V_c) \times V_c \tag{7}$$

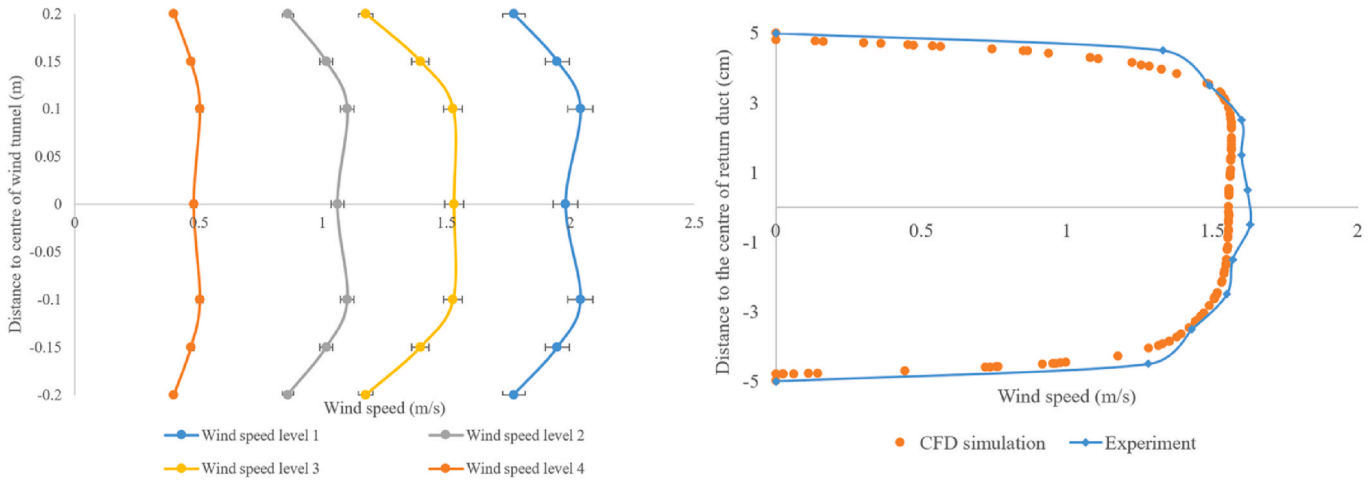

(a) Wind tunnel outlet (b) Return duct

Fig. 11. Wind speed profile in the (a) open wind tunnel outlet and (b) return duct, comparing CFD results against experimental measurements.

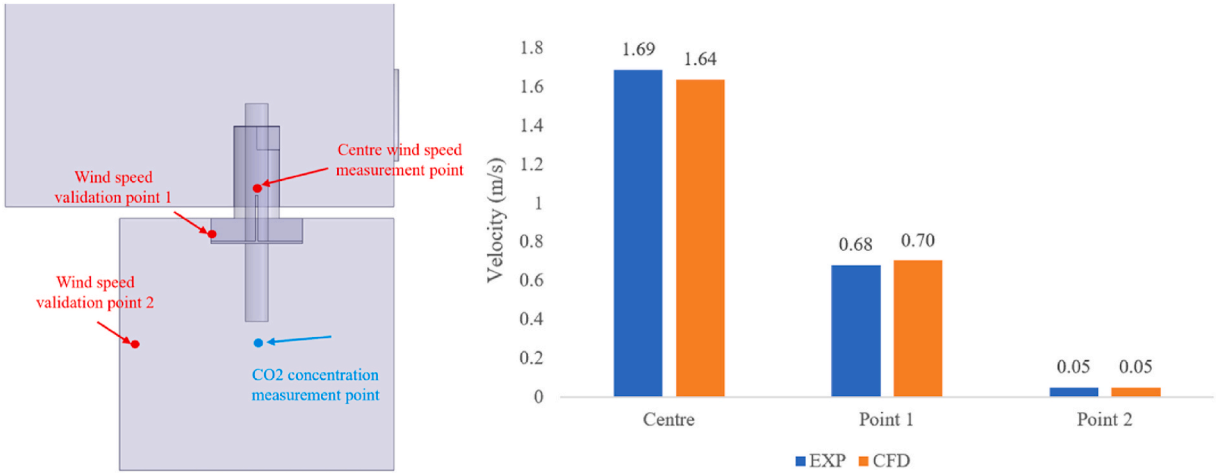

Fig. 12. Validation of the airflow velocity predictions using measured airflow velocity at different points.

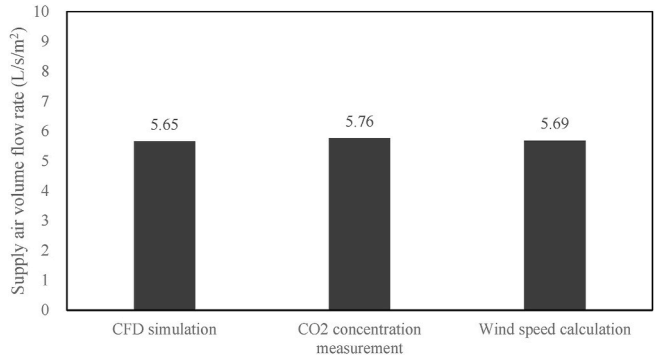

Fig. 13. Windcatcher ventilation rate from different measurement methods.

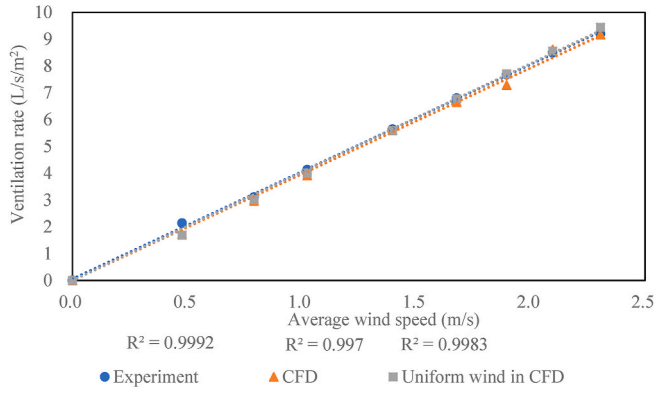

Fig. 14. Scaled windcatcher ventilation performance: comparison between CFD and experimental results.

The ventilation rate was calculated using Equation (8):

$$Q = \overline{V} \times A = (0.9627 - 0.022 \times V_c) \times V_c \times A = -0.00017 \times V_c^2 + 0.00756 \times V_c \quad (8)$$

The wind speeds measured from the experiment and predicted by the CFD simulation at three different points in the test room were compared for the CFD model validation, as shown in Fig. (12). The wind speed at three points slightly fluctuated because of the accuracy of the sensor and the turbulence of the wind, but the average wind velocity in the three points could match the CFD simulation. The relationship between validation point 1 to the centre wind speed measurement point was about 0.45 times the centre velocity.

The air change rate of the test room was also estimated by the carbon dioxide concentration change rate, as shown in Fig. (13), wind speed in the return duct and the CFD simulation, the maximum difference between each method was about 0.1L/s, which was ignorable for the ventilation rate evaluation of the windcatcher.

The simulation method was validated by three different methods, including the carbon dioxide concentration change rate, wind speed profile in the return duct and the wind speed at a different location in the test room. Generally, a good agreement was observed between different approaches.

4.2. Ventilation performance of the scaled experimental model

Fresh air was supplied between 1.7 L/s/m^2 and 9.18 L/s/m^2 for an outdoor wind speed of 0.5 m/s to 2.5 m/s, in the scaled prototype. The average ventilation rate difference between the CFD simulation and experiment was 0.156L/s/m^2 or an average difference of 4.5%. A linear relationship between average wind speed and ventilation rate was observed. The difference between the ventilation rate predicted by the CFD model, which employed the wind profile from the open wind tunnel and a uniform wind environment, was minimal.

In the evaluation of the rotation, the wind scoop could face the wind at a wind speed of 1 m/s and higher. The wind scoop would rotate fast at the beginning and stop slowly as the torque was higher when the angle of the wind to the vertical tail fin was large. The wind scoop would not fluctuate at the final place because of the friction and low torque at the final position. With the development of a commercial prototype, the wind speed required to rotate should be further decreased. The movement of the rotating wind scoop under 1 m/s wind is shown in Fig. (15) and Video 1. It shows that the angle change in the first 3 s was large and stopped slowly as it faced the wind steadily in the last 3 s.

Supplementary Video 1 related to this article can be found at https://doi.org/10.1016/j.buildenv.2023.110018

As shown in the pressure contour in Fig. (16), the biggest pressure loss in the system was observed in the return duct. In the validated scaled model, the supply and return duct cross-section areas were not perfectly balanced, because of the manufacturing constraints, resulting in a higher airflow velocity in the return duct and a higher pressure loss, compared to the full-scale model in Fig. (19) in Section 4.3. As shown in Fig.(16), the return duct was extended into the room to increase the distance between the wind speed measurement point and the inlet of the return duct which reduced the airflow velocity difference between the

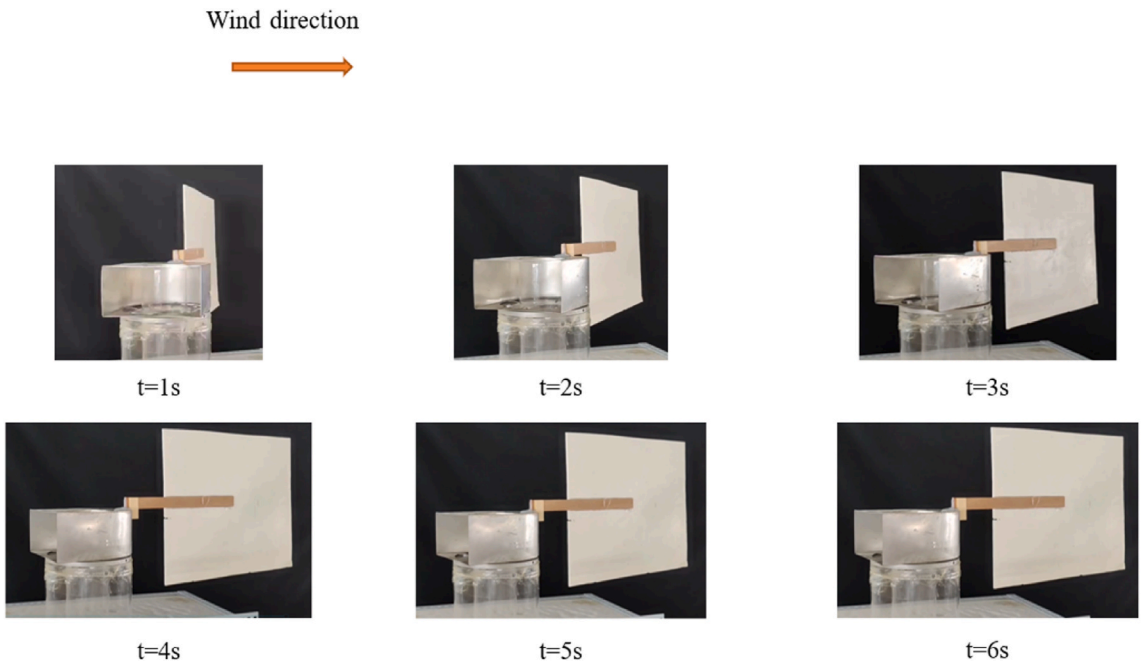

Fig. 15. Snapshots of the rotation of the wind scoop windcatcher device. You can view the video here: https://doi.org/10.1016/j.buildenv.2023.110018

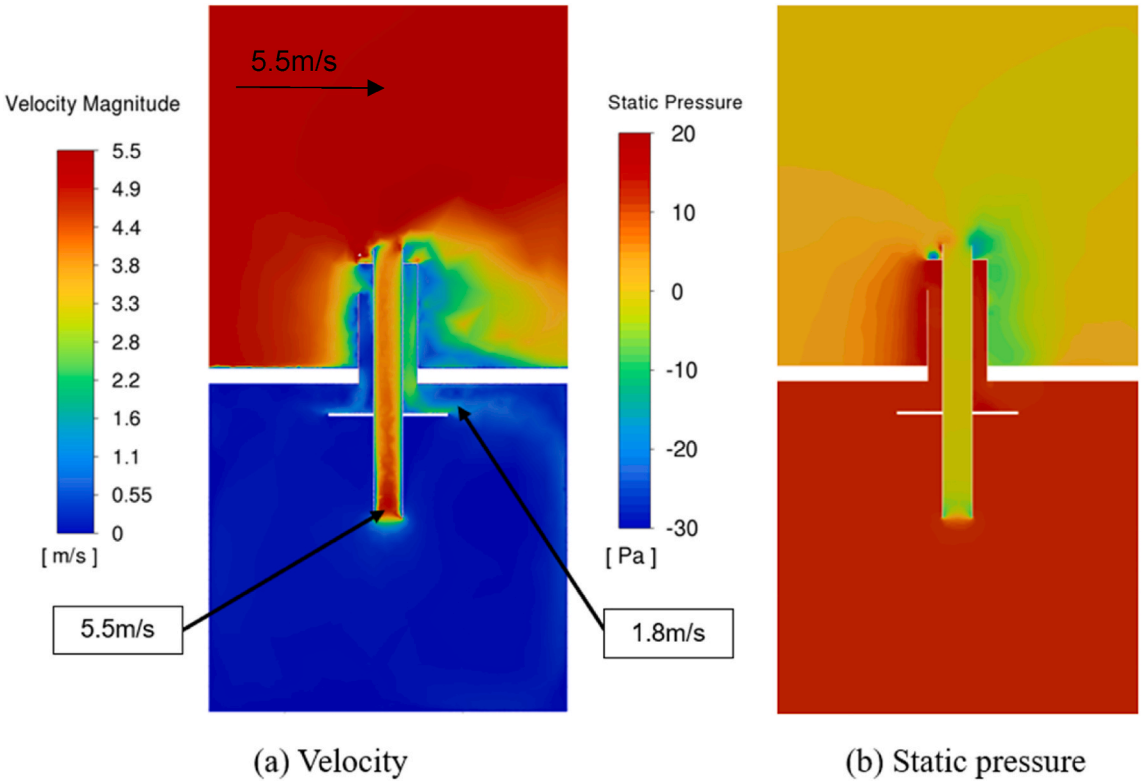

Fig. 16. Cross-sectional contours showing the velocity and static pressure distribution in the scaled wind catcher model, outdoor wind speed at 5.5 m/s.

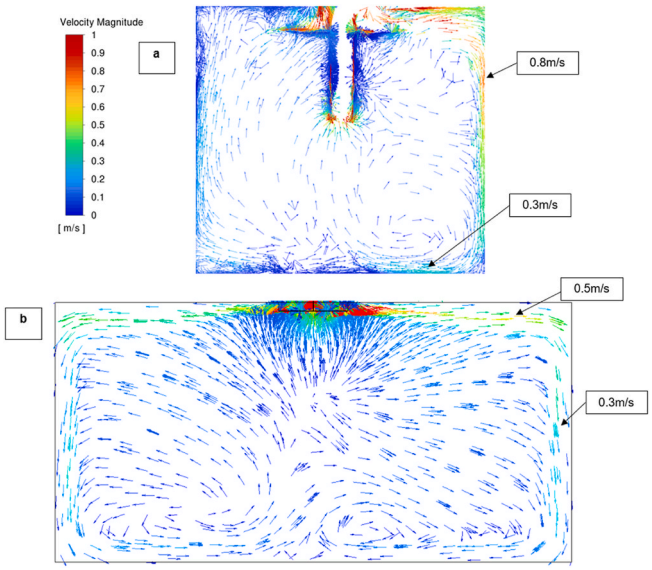

Fig. 17. Air circulation inside the room at 5 m/s environment wind speed (a) experiment model (b) full-scale model.

middle and the side. The airflow in the return duct was more uniform after entering and as it flows into the return duct. However, the extension of the return duct also increased the pressure loss of the system which will be modified in the full-scale model.

The air was diffused by the anti-short circuit device and the velocity of airflow at the occupancy level in the room was lower than 0.5 m/s at 5 m/s outdoor wind speed, which would not cause discomfort and air draught. The correct airflow direction was achieved and the indoor air was circulated well when the ASCD was added as shown in Fig. (17). The wind speed on the two sides was not identical in the experiment model as the outdoor wind came from the left side but the wind speed in the highest part of the room was still lower than 1 m/s at 5 m/s environment wind speed. The supply and exhaust ventilation was achieved aided by the pressure differences between the inlet and outlet.

4.3. Ventilation performance of the full-scale windcatcher model

For the full-scale model, the overall diameter of the windcatcher was increased from 200 mm to 450 mm, and the size of the test room was increased to 6 m × 6 m × 3 m. The increase of the windcatcher size effectively increased the ventilation rate in the same wind conditions. However, it should be noted that the room volume also increased to 108 m^3, and hence a larger volume is ventilated. As observed, a linear relationship between the ventilation rate and outdoor wind speed was achieved (see Fig. 18). The full-scale rotary scoop windcatcher could provide a ventilation rate from 32 L/s to 226 L/s at 1–7 m/s environment wind speed. The fresh air supply at low outdoor wind speed conditions was over 30 L/s which was sufficient for three occupants, according to the requirement of 10 L/s/person in CIBSE Guide A for occupants working in an office [49]. Considering the windcatcher was normally placed on the top of a building with a higher environment

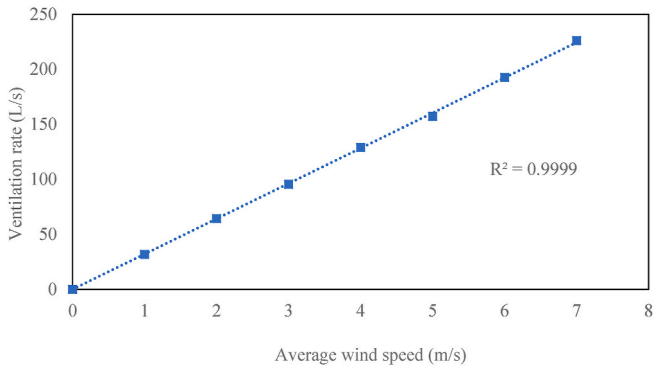

Fig. 18. Impact of outdoor wind speed on the ventilation rate of the full-scale windcatcher model.

wind speed, the windcatcher with 450 mm diameter could provide sufficient fresh air supply for commercial use and a damper is necessary to avoid over-ventilation.

As shown in Fig. (19), the wind speed in the return duct in the full-scale model was lower than the initial scaled model at the same outdoor wind speed. Although the airflow velocity was decreased from 5.5 m/s to 3.5 m/s in the return duct under the same environment wind speed, the section area was increased, and the overall ventilation rate was increased. The size of the full-scale windcatcher was about 2.25 times larger than the scaled model but the ventilation rate in the full-scale model was over five times of the scaled model. The airflow from the two sides of the ASCD was also more balanced than in the scaled model. After reaching the side wall of the room, the airflow was diffused in different directions and the airflow velocity was decreased from 1.8 m/s to about 0.3 m/s close to the wall and the occupancy level.

In the pressure contour, the static pressure in the outside environment was identical to the initial condition but the internal pressure in the full-scale model was lower than the initial scale model, which was caused by the lower pressure loss in the return duct in the full-scale building. .

4.4. Comparison with a conventional windcatcher device

In order to demonstrate further the capabilities of the proposed windcatcher, its ventilation performance was compared with aconventional windcatcher. In a conventional two or three-sided windcatcher, the ventilation rate was sensitive to the wind direction, but increasing the opening number could decrease the effect of changing wind directions [41]. Thus, an eight-sided windcatcher was selected to closely compare with the rotary windcatcher in this research.

As observed in Fig. (20), the ventilation performance of the rotary wind scoop windcatcher is slightly higher, about 10%, than the conventional eight-side windcatcher as the inlet area facing the wind with high positive pressure, and the outlet was on the top with a high negative pressure which resulted in a higher pressure difference between inlet and outlet.

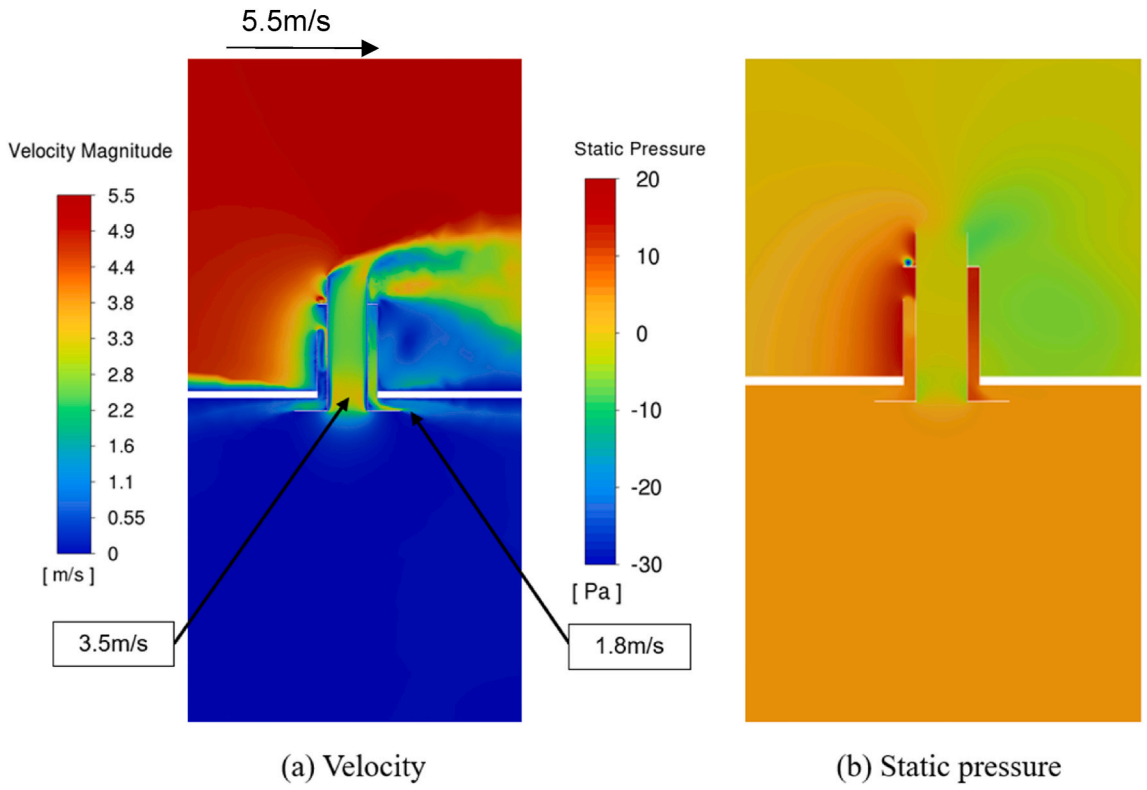

Fig. 19. Cross-sectional contours showing the velocity and static pressure distribution in the full-scale wind catcher model, outdoor wind speed at 5.5 m/s.

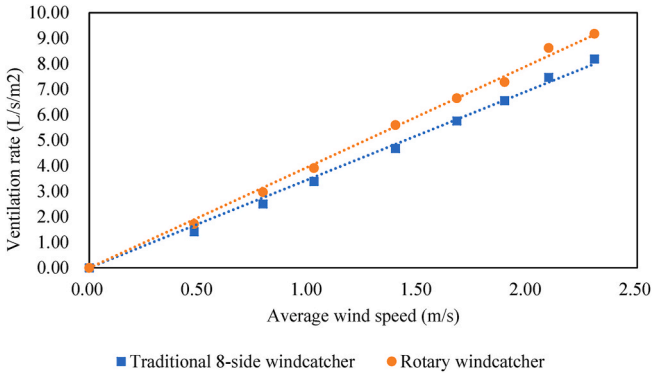

Fig. 20. Comparison of conventional windcatcher and full-scale rotary scoop windcatcher.

5. Discussions

The present study proposed a windcatcher which contained a supply wind scoop and a return central chimney. The application of the rotary windcatcher system only required one opening on the roof structure for both supply and return ductwork, reducing the complexity and installation cost. The connections and seams between the roof structure and the rooftop equipment would not only increase the cost of the construction and maintenance but also increase the risk of water leakage (for example in the case of applying a heat pipe cooling strategy) and airtightness issues.

Like the prototype, the windcatcher device surfaces could be constructed using transparent or glass material which could also provide daylighting to the room. The rotary wind scoop and tail fin could also be made of transparent materials to allow the light to pass through. The impact of this on daylighting performance should be explored. A damper will be necessary for commercial applications to control the ventilation rate during high outdoor wind speed conditions to avoid discomfort and overventilation.

In the present research, the fixed supply and return channels were achieved. The airflow inside the ventilation system was similar to that of a mechanical ventilation system but the fans were replaced by natural wind power to save energy. Thus, passive/low-energy devices could be applied effectively with the proposed windcatcher. Cooling devices could be added to the supply channel to reduce the temperature of the supply air or moisture in the supply air. Heat recovery devices such as heat pipes could be applied, and the heat could be transferred from the return air to the supply air continuously without the impact of changing wind directions (Figure A1 and A2). The moisture could be absorbed from the supply air and emitted to the return air with appropriate design in further research. So the dehumidification could also be achieved by passive dehumidification technqiues such as the use of silica gel [50]. Passive heating using solar energy could also be applied in the supply duct such as a solar wall. And the evaporative cooling device could be installed in the supply channel.

In the current research, the ventilation performance of the windcatcher was investigated numerically and experimentally only considering the horizontal wind to simplify. However, the application of windcatcher in cities or urban areas is much more complex, especially in large cities with high-rise buildings, where the vertical wind need to be considered in the research [51]. The solar radiation on the wall surface would also influence the vertical flow and the buoyancy effect which has to be taken into account in the actual application of the windcatcher [52]. Thus, the vertical flow and the temperature conditions need to be considered in further research including both CFD simulation and field study of the windcatcher.

The rotary wind scoop windcatcher was designed for different types of passive technology integrations. However, we only presented the initial concept and focused on the ventilation performance in the present work. The performance of the different passive cooling and heating integration with the proposed windcatcher will be explored in future research. Initial results of the rotary wind scoop and heat recovery

modelling is presented in the Appendix. Figure A1 and A2 shows the example application of the proposed technology and could help visualize the operation of the windcatcher with heat recovery.

It should be noted that the current experiment prototype was not a fully airtight rotary windcatcher. Thus, in the research, the experiment model was simplified and adjusted by removing the ring-shaped bearing for the ventilation rate testing and removing the extended chimney for the rotation test. The geometry of this prototype and the components inside need to be further optimized for both ventilation performance and rotation performance for further application.

6. Conclusions and future works

In this research, a novel dual-channel wind scoop windcatcher was developed for capturing wind flow in changing wind directions and providing a stable fresh air supply in the fixed supply and exhaust air in the return duct. This windcatcher addresses the issue of the incorporation of passive heating and cooling technologies in conventional windcatchers. With the fixed and adjacent supply and return channels which were not affected by the changing wind direction, passive technologies can be applied in this windcatcher, such as solar heating and heat recovery. The prototype of the windcatcher and an open wind tunnel and test room were constructed for the evaluation of the ventilation performance. The simplified wind tunnel contained a contraction to increase the wind speed and a flow conditioners to stabilize the wind. The test room airtightness was 0.0625 h^{-1}, evaluated by the tracer-gas decay method using carbon dioxide.

The ventilation rate under different wind speeds was also evaluated by airspeed measurement and tracer-gas decay method.

The wind speed at different points in the test room and the ventilation rate in the CFD model were validated with the experiment results. The wind speed in the centre of the return duct was measured at different outdoor wind speeds for the ventilation rate estimation. The average difference between the ventilation rate in the CFD model and the experiment results was 4.5%, and most of the differences were lower than 2%.

The validated experiment prototype was modified into a full-scale model in CFD to further evaluate the fresh air supply rates, airflow velocity and pressure distribution. The application of the anti-short circuit device (ASCD) also improved the air circulation in the ventilated space. Fresh air was supplied by the windcatcher device between 1.7 L/s/m^2 and 9.18 L/s/m^2 for an outdoor wind speed of 0.5 m/s to 2.5 m/s in the scaled experiment prototype. And the full-scale rotary scoop windcatcher could provide a ventilation rate from 32 L/s to 226 L/s at 1–7 m/s environment wind speed. The ventilation rate was 10% higher than that of a conventional eight-side windcatcher under the same environment wind speed with the same size. The current minimum wind speed to rotate the wind scoop prototype was 1 m/s which should be further improved in future research.

Tthe experiment and CFD simulations only considered the windcatcher operation under horizontal wind without any internal heat gains. The buoyancy effect at low wind speed conditions and the impact of vertical wind needs to be considered in further research. The rotation part in the prototype needs to be further optimized to reduce the minimum wind speed for rotation and improve air tightness. In future research, the geometry of the windcatcher can be further optimized, and the passive heating, cooling, dehumidification, and energy recovery technologies should be applied in the fixed supply and return duct. Passive heating using solar and passive cooling using evaporative or absorption cooling should be investigated by experiment and field study, and the passive dehumidification method should be evaluated. The ventilation performance of the full-scale windcatcher should be evaluated in a larger wind tunnel and field test in further research. The optimization of the rotary wind scoop in the windcatcher also needs to be investigated to decrease the capital and maintenance cost of the windcatcher.

CRediT authorship contribution statement

Jiaxiang Li: Writing – original draft, Visualization, Validation, Software, Resources, Methodology, Investigation, Funding acquisition, Formal analysis, Data curation, Conceptualization. **John Calautit:** Writing – review & editing, Supervision, Methodology. **Carlos Jimenez-Bescos:** Supervision. **Saffa Riffat:** Writing – review & editing.

Declaration of competing interest

The authors declare that they have no known competing financial interests or personal relationships that could have appeared to influence the work reported in this paper.

Data availability

The data that has been used is confidential.

Acknowledgement

Thanks to the support of Dalian Meizhu furniture Co., Ltd for the assistance in making the experiment model and providing the test space.

Appendix

Table A1
Wind speed function

Average wind speed (m/s)	Wind speed profile function (m/s)
2.31	$v = -48.2 \times r^2 + 7.7 \times r + 2.33$
2.10	$v = -42.8 \times r^2 + 6.3 \times r + 2.27$
1.90	$v = -16.4 \times r^2 + 2.2 \times r + 1.98$
1.68	$v = -27.2 \times r^2 + 3.8 \times r + 1.79$
1.40	$v = -17.4 \times r^2 + 1.7 \times r + 1.53$
1.03	$v = -14.1 \times r^2 + 1.8 \times r + 1.07$
0.79	$v = -8.2 \times r^2 + 1.2 \times r + 0.81$
0.48	$v = -6.5 \times r^2 + 0.9 \times r + 0.49$

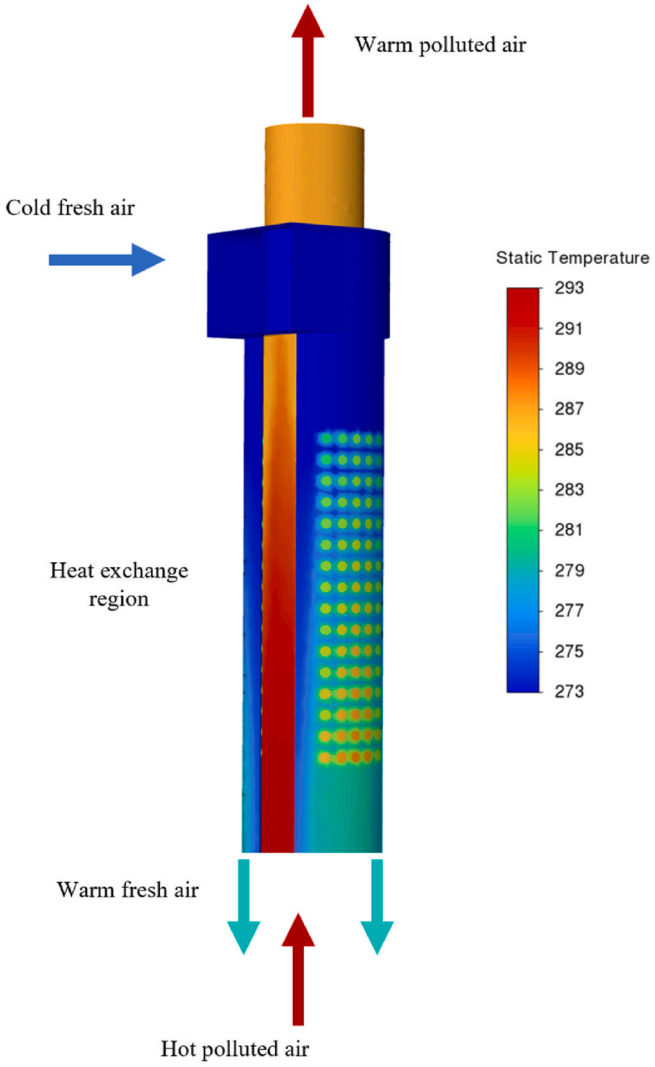

Fig. A1. Example contour of heat recovery in the rotary scoop windcatcher

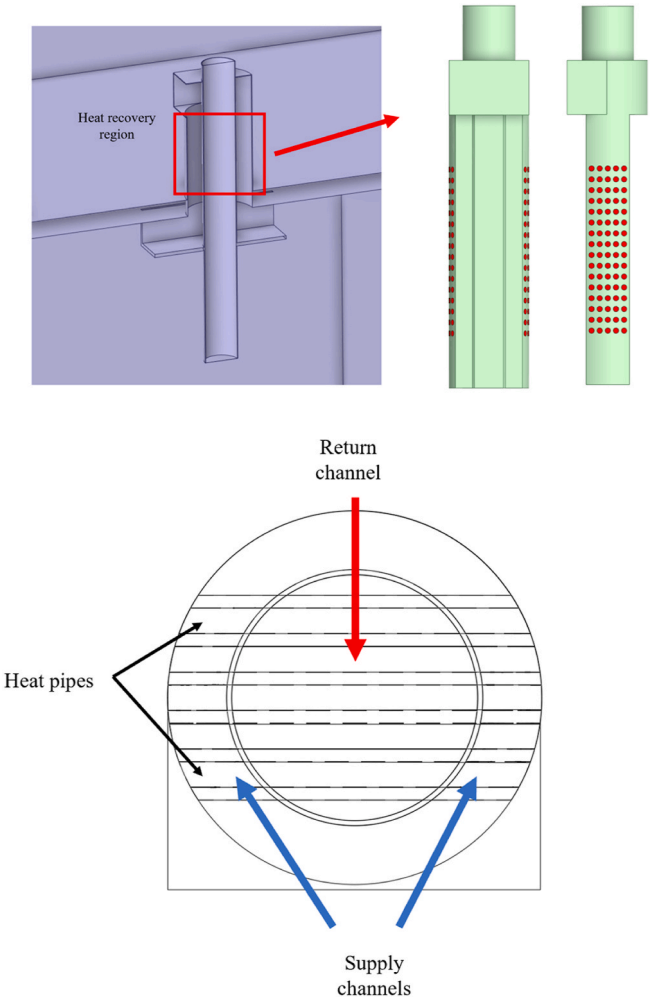

Fig. A2. Location and layout example of the heat recovery in windcatcher

References

[1] O. Saadatian, et al., Review of windcatcher technologies, Renew. Sustain. Energy Rev. 16 (3) (2012) 1477–1495.
[2] B.-j. He, et al., Overview of rural building energy efficiency in China, Energy Pol. 69 (2014) 385–396.
[3] C.J. Rhodes, The 2015 Paris climate change conference: Cop21, Sci. Prog. 99 (1) (2016) 97–104.
[4] M. Fan, et al., A review of different ventilation modes on thermal comfort, air quality and virus spread control, Build. Environ. 212 (2022), 108831.
[5] L. Pérez-Lombard, J. Ortiz, C. Pout, A review on buildings energy consumption information, Energy Build. 40 (3) (2008) 394–398.
[6] IEA, The Future of Cooling-Opportunities for Energy-Efficient Air Conditioning, 2018.
[7] H.-Y. Chan, S.B. Riffat, J. Zhu, Review of passive solar heating and cooling technologies, Renew. Sustain. Energy Rev. 14 (2) (2010) 781–789.
[8] F. Jomehzadeh, et al., Natural ventilation by windcatcher (Badgir): a review on the impacts of geometry, microclimate and macroclimate, Energy Build. 226 (2020), 110396.
[9] N.Z. Ghalam, M. Farrokhzad, H. Nazif, Investigation of optimal natural ventilation in residential complexes design for temperate and humid climates, Sustainable Energy, Grids and Networks 27 (2021), 100500.
[10] N. Nasrollahi, P. Ghobadi, Field measurement and numerical investigation of natural cross-ventilation in high-rise buildings; Thermal comfort analysis, Appl. Therm. Eng. 211 (2022), 118500.
[11] E. Bay, A. Martinez-Molina, W.A. Dupont, Assessment of natural ventilation strategies in historical buildings in a hot and humid climate using energy and CFD simulations, J. Build. Eng. 51 (2022), 104287.
[12] P. Liu, M. Justo Alonso, H.M. Mathisen, Heat recovery ventilation design limitations due to LHC for different ventilation strategies in ZEB, Build. Environ. 224 (2022), 109542.
[13] K. Bamdad, et al., SIntroducing Extended Natural Ventilation Index for Buildings under the Present and Future Changing Climates, Building and Environment, 2022, 109688.
[14] P.K. Sangdeh, N. Nasrollahi, Windcatchers and their applications in contemporary architecture, Energy and Built Environment 3 (1) (2022) 56–72.
[15] Y. He, et al., Experimental and CFD study of ventilation performance enhanced by roof window and mechanical ventilation system with different design strategies, Build. Environ. 224 (2022), 109566.
[16] H. Montazeri, R. Azizian, Experimental study on natural ventilation performance of one-sided wind catcher, Build. Environ. 43 (12) (2008) 2193–2202.
[17] W. Pan, et al., A model for calculating single-sided natural ventilation rate in an urban residential apartment, Build. Environ. 147 (2019) 372–381.
[18] Z. Moghtader Gilvaei, A. Haghighi Poshtiri, A. Mirzazade Akbarpoor, A novel passive system for providing natural ventilation and passive cooling: evaluating thermal comfort and building energy, Renew. Energy 198 (2022) 463–483.
[19] M. Afshin, et al., An experimental study on the evaluation of natural ventilation performance of a two-sided wind-catcher for various wind angles, Renew. Energy 85 (2016) 1068–1078.
[20] L. Moosavi, et al., New Design for Solar Chimney with Integrated Windcatcher for Space Cooling and Ventilation, vol. 181, Building and Environment, 2020, 106785.
[21] L. Li, C.M. Mak, The assessment of the performance of a windcatcher system using computational fluid dynamics, Build. Environ. 42 (3) (2007) 1135–1141.
[22] B.M. Jones, R. Kirby, Quantifying the performance of a top–down natural ventilation Windcatcher™, Build. Environ. 44 (9) (2009) 1925–1934.
[23] M. Liu, C. Jimenez-Bescos, J. Calautit, CFD investigation of a natural ventilation wind tower system with solid tube banks heat recovery for mild-cold climate, J. Build. Eng. 45 (2022), 103570.
[24] J.K. Calautit, D. O'Connor, B.R. Hughes, A natural ventilation wind tower with heat pipe heat recovery for cold climates, Renew. Energy 87 (2016) 1088–1104.
[25] J.K. Calautit, et al., Development of a natural ventilation windcatcher with passive heat recovery wheel for mild-cold climates: CFD and experimental analysis, Renew. Energy 160 (2020) 465–482.

[26] M. Farouk, Comparative study of hexagon & square windcatchers using CFD simulations, J. Build. Eng. 31 (2020), 101366.
[27] S. Jafari, V. Kalantar, Numerical simulation of natural ventilation with passive cooling by diagonal solar chimneys and windcatcher and water spray system in a hot and dry climate, Energy Build. 256 (2022), 111714.
[28] M. Ghoulem, et al., Analysis of passive downdraught evaporative cooling windcatcher for greenhouses in hot climatic conditions: Parametric study and impact of neighbouring structures, Biosyst. Eng. 197 (2020) 105–121.
[29] A. Noroozi, Y. Veneris, Thermal assessment of a novel combine evaporative cooling wind catcher, Energies 11 (2018) 442.
[30] Z.M. Gilvaei, A.H. Poshtiri, A.M. Akbarpoor, A Novel Passive System for Providing Natural Ventilation and Passive Cooling: Evaluating Thermal Comfort and Building Energy, Renewable Energy, 2022.
[31] K. Pelletier, J. Calautit, Analysis of the performance of an integrated multistage helical coil heat transfer device and passive cooling windcatcher for buildings in hot climates, J. Build. Eng. 48 (2022), 103899.
[32] N. Kumar, et al., Parametric study on vertical void configurations for improving ventilation performance in the mid-rise apartment building, Build. Environ. 215 (2022), 108969.
[33] B. Zhang, et al., Turbulence-induced ventilation of an isolated building: ventilation route identification using spectral proper orthogonal decomposition, Build. Environ. 223 (2022), 109471.
[34] J.K. Calautit, B.R. Hughes, S.S. Shahzad, CFD and wind tunnel study of the performance of a uni-directional wind catcher with heat transfer devices, Renew. Energy 83 (2015) 85–99.
[35] J.K. Calautit, B.R. Hughes, A passive cooling wind catcher with heat pipe technology: CFD, wind tunnel and field-test analysis, Appl. Energy 162 (2016) 460–471.
[36] J.P. Harrouz, K. Ghali, N. Ghaddar, Integrated solar – windcatcher with dew-point indirect evaporative cooler for classrooms, Appl. Therm. Eng. 188 (2021), 116654.
[37] H. Montazeri, et al., Two-sided wind catcher performance evaluation using experimental, numerical and analytical modeling, Renew. Energy 35 (7) (2010) 1424–1435.
[38] J.K. Calautit, et al., Numerical and experimental investigation of the indoor air quality and thermal comfort performance of a low energy cooling windcatcher with heat pipes and extended surfaces, Renew. Energy 145 (2020) 744–756.
[39] N. Khan, et al., Performance testing and comparison of turbine ventilators, Renew. Energy 33 (11) (2008) 2441–2447.
[40] N. Khan, Y. Su, S.B. Riffat, A review on wind driven ventilation techniques, Energy Build. 40 (8) (2008) 1586–1604.
[41] M. Farouk, Comparative study of hexagon & square windcatchers using CFD simulations, J. Build. Eng. (2020) 31.
[42] P. Nejat, et al., Anti-short-circuit device: a new solution for short-circuiting in windcatcher and improvement of natural ventilation performance, Build. Environ. 105 (2016) 24–39.
[43] J.H. Bell, R.D. Mehta, Design and Calibration of the Mixing Layer and Wind Tunnel, 1989.
[44] S. Kirk, M. Kolokotroni, Windcatchers in modern UK buildings: experimental study, Int. J. Vent. 3 (1) (2004) 67–78.
[45] P.S. Charlesworth, Air Exchange Rate and Airtightness Measurement Techniques - an Application Guide, Coventry: Air Infiltration and Ventilation Centre, 1988.
[46] T. Kobayashi, et al., Numerical Analysis of Wind-Induced Natural Ventilation for an Isolated Cubic Room with Two Openings under Small Mean Wind Pressure Difference, Building and Environment, 2022, 109694.
[47] B.R. Hughes, J.K. Calautit, S.A. Ghani, The development of commercial wind towers for natural ventilation: a review, Appl. Energy 92 (2012) 606–627.
[48] P. Kheirkhah, N. Nasrollahi, Windcatchers and Their Applications in Contemporary Architecture, vol. 3, Energy and Built Environment, 2020.
[49] X. Chen, et al., Recent progress in liquid desiccant dehumidification and air-conditioning: a review, Energy and Built Environment 1 (1) (2020) 106–130.
[50] H. Lee, et al., A fundamental study of intelligent building envelope systems capable of passive dehumidification and solar heat collection utilizing renewable energy, Energy Build. 195 (2019) 139–148.
[51] Y. Fan, et al., Diurnal variation of natural convective wall flows and the resulting air change rate in a homogeneous urban canopy layer, Energy Build. 153 (2017) 201–208.
[52] Y. Fan, et al., Natural convection flows along a 16-storey high-rise building, Build. Environ. 107 (2016) 215–225.